



## Measurement of the muon charge asymmetry in $p\bar{p} \rightarrow W + X \rightarrow \mu\nu + X$ events using the DØ detector

The DØ Collaboration  
(Dated: August 26, 2009)

We present preliminary results of a measurement of the muon production charge asymmetry from  $W \rightarrow \mu\nu$  decay using  $4.9 \text{ fb}^{-1}$  of data collected with the DØ detector. The measured asymmetries for muon pseudorapidity  $|\eta| < 2$  are compared with the theory prediction using the CTEQ6.6 PDF set. The total uncertainties are smaller than the PDF uncertainties in most  $\eta$  bins.

*Preliminary Results for Lepton-Photon 2009*

## I. INTRODUCTION

In  $p\bar{p}$  collisions, production of  $W^\pm$  bosons mainly happens between valence  $u(\bar{u})$  and valence  $\bar{d}(d)$  quarks:

$$\begin{aligned} u + \bar{d} &\rightarrow W^+ \rightarrow \mu^+ + \nu_\mu \\ \bar{u} + d &\rightarrow W^- \rightarrow \mu^- + \bar{\nu}_\mu \end{aligned}$$

As the  $u$  quark tends to carry a higher proton momentum fraction than the  $d$  quark does, the  $W^+(W^-)$  boson is generally produced with momentum along the proton(antiproton) direction.

The  $W$  production asymmetry is defined as

$$A(y_W) = \frac{d\sigma(W^+)/dy_W - d\sigma(W^-)/dy_W}{d\sigma(W^+)/dy_W + d\sigma(W^-)/dy_W} \quad (1)$$

where  $y_W$  is the rapidity of the  $W$  boson, defined as

$$y_W = \frac{1}{2} \ln \left( \frac{E + p_z}{E - p_z} \right) \quad (2)$$

where  $E$  and  $p_z$  are the energy and momentum in the  $z$  direction of the  $W$  boson, respectively.

The momentum fraction of the proton (antiproton) carried by the  $u$  or  $d$  quark is related to the  $W$  boson rapidity as

$$x_{u,d} = \frac{M_W}{\sqrt{s}} e^{\pm y_W} \quad (3)$$

where  $s$  is the center-of-mass energy of the  $p\bar{p}$  collision, and the  $+(-)$  sign is used for the  $u$  ( $d$ ) quark.

Experimentally, neutrinos pass through detector materials without interactions. Therefore, the momentum in the  $z$  direction of the  $W$  boson cannot be measured directly. We measure, instead, the charge asymmetry of muons from  $W \rightarrow \mu\nu$  decays. The charge asymmetry of the muon results from the  $W$  boson asymmetry convoluted with the V-A decay of the  $W$  boson to  $\mu\nu$ . The muon charge asymmetry is calculated as

$$A(\eta) = \frac{d\sigma(\mu^+)/d\eta - d\sigma(\mu^-)/d\eta}{d\sigma(\mu^+)/d\eta + d\sigma(\mu^-)/d\eta} \quad (4)$$

where  $\eta$  is the muon pseudorapidity depending on the polar angle  $\theta$ ,  $\eta = -\ln[\tan(\theta/2)]$ , and  $\eta \approx y$  at high energy.

The cross section for  $W \rightarrow \mu\nu$  decay can be measured as

$$\frac{d\sigma(\mu)}{d\eta} = \frac{N_\mu(\eta)}{\mathcal{L}\mathcal{A}(\eta)\epsilon(\eta)} \quad (5)$$

where  $\epsilon$  is the efficiency to measure muons,  $\mathcal{L}$  is the integrated luminosity of  $p\bar{p}$  collisions,  $\mathcal{A}$  is the detector acceptance, and  $N_\mu$  is the number of muons in a given  $\eta$  bin. If the integrated luminosity, detector acceptance, and efficiencies are independent of the muon charge, the muon charge asymmetry can be written as

$$A(\eta_\mu) = \frac{N_{\mu^+}(\eta) - N_{\mu^-}(\eta)}{N_{\mu^+}(\eta) + N_{\mu^-}(\eta)} \quad (6)$$

Figure 1 shows the theory prediction of  $W$  production asymmetry and muon charge asymmetry in different  $W$   $p_T$  and muon  $p_{T,\mu}$  regions. The muon charge asymmetry is dominated by the V-A decay asymmetry at high rapidity and low  $p_{T,\mu}$ . At high  $p_{T,\mu}$ , the asymmetry from  $W$  production becomes the principal contribution. The muon charge asymmetry is also sensitive to the momentum of the  $W$  boson.

## II. DØ DETECTOR

At the Tevatron, protons and antiprotons collide at a center of mass energy of 1.96 TeV. The DØ detector is built concentrically around the beampipe. It consists of a central tracking system, a calorimeter, and a muon system.

Closest to the beamline and located within a 2 T superconducting solenoidal magnet is the central tracking system, including the silicon microstrip tracker (SMT) and the central fiber tracker (CFT). The SMT provides a high resolution

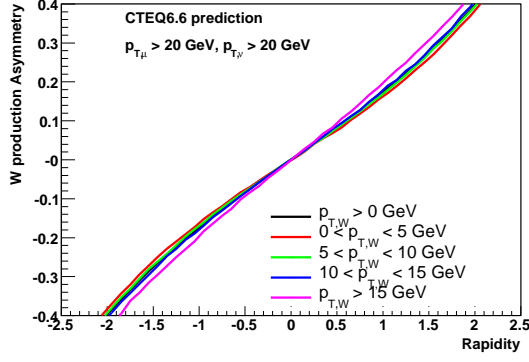
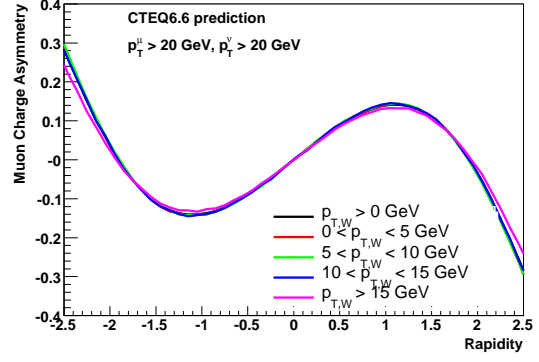
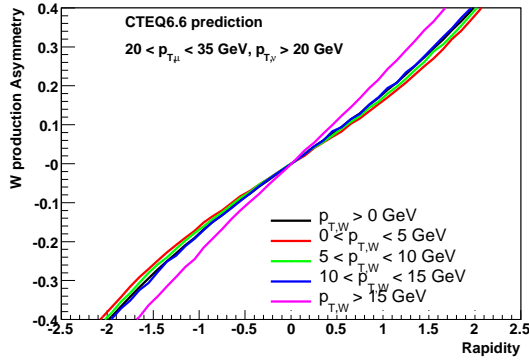
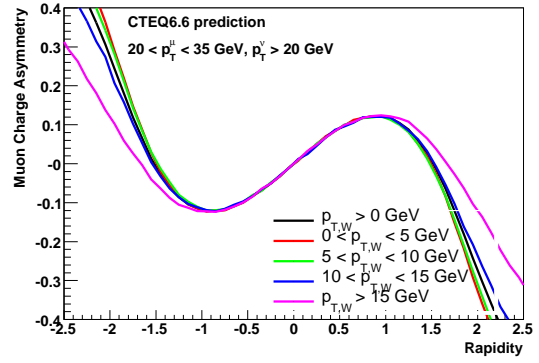
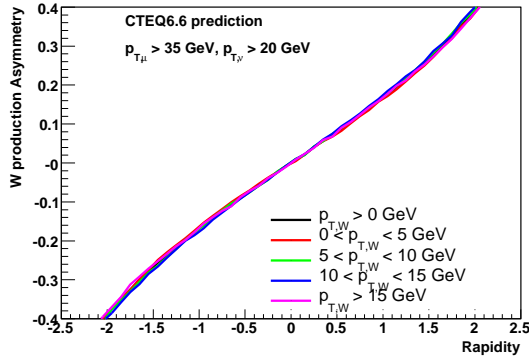
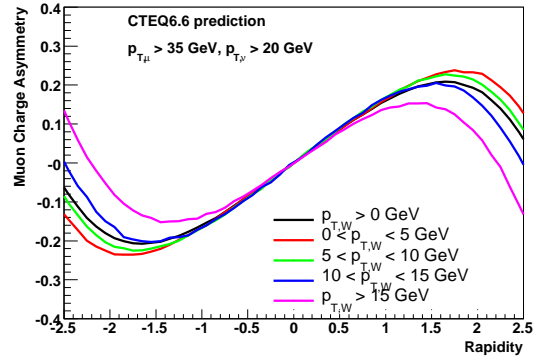
(a)  $W$  production asymmetry,  $p_{T,\mu} > 20$  GeV(b) Muon charge asymmetry,  $p_{T,\mu} > 20$  GeV(c)  $W$  production asymmetry,  $20 < p_{T,\mu} < 35$  GeV(d) Muon charge asymmetry,  $20 < p_{T,\mu} < 35$  GeV(e)  $W$  production asymmetry,  $p_{T,\mu} > 35$  GeV(f) Muon charge asymmetry,  $p_{T,\mu} > 35$  GeV

FIG. 1: Theory prediction of  $W$  production asymmetry and muon charge asymmetry in different  $W$   $p_T$  ranges: above 0 GeV (blue), 0-5 GeV (red), 5-10 GeV (green), 10-15 GeV (cyan), and above 15 GeV (pink). The top row is the predictions for muons with  $p_{T,\mu} > 20$  GeV, center row is for  $20 < p_{T,\mu} < 35$  GeV, and the bottom row is for  $p_{T,\mu} > 35$  GeV.

position measurement and serves to reconstruct tracks of charged particles near the beam line. The large size of the CFT helps track particles over a long distance.

Enclosing the central tracking system is the calorimeter. The calorimeter uses multiple layers of uranium in liquid argon to measure the energies of particles. It has a central section and two end caps covering the central, forward and backward regions.

Outermost is the muon detector. It consists of three layers of scintillator for triggering and wire chambers for coordinate measurement. The innermost layer, lies inside a toroid. The calorimeter supports make a hole in the region  $|\eta| < 1.25$ ,  $4.25 < \phi < 5.15$  in the coverage for muons, where  $\phi$  is the azimuthal angle.

The magnet polarities of the  $D\bar{O}$  detector are frequently reversed to avoid any asymmetry of the detector.

### III. DATA SAMPLES AND EVENT SELECTION

The data used in this analysis were collected between April 2002 and April 2009 and have a total integrated luminosity  $\approx 4.9 \text{ fb}^{-1}$ . Data were collected during two running periods, Run IIa and Run IIb. For this analysis, the primary difference between the two periods is the increased instantaneous luminosity of Run IIb resulting in reduced trigger coverage for Run IIb. Data from each running period were analyzed independently, with the results combined to provide a single measurement of the muon asymmetry.

We use events which satisfied any of several single muon triggers covering the pseudorapidity range  $|\eta_{\text{det}}| < 1.6$ , where  $\eta_{\text{det}}$  is the pseudorapidity measured with respect to the center of the detector. A second set of single muon triggers covering  $|\eta_{\text{det}}| < 2$  was available during Run IIa; these were used to select events passing  $1.6 < |\eta_{\text{det}}| < 2$ . In addition, events must satisfy the following requirements:

1. contain a muon matched to a central track with transverse momentum  $p_T > 20 \text{ GeV}$  satisfying the following conditions:
  - the track has at least one hit in the SMT;
  - the distance of closest approach,  $dca$ , of the track to the beam position in the  $x$ - $y$  plane satisfies  $|dca| < 0.02 \text{ cm}$ ;
  - $\chi^2/\text{dof} < 4.0$ , where  $\chi^2$  and the number of degrees of freedom (dof) are global fit parameters of the central track;
  - the track must match a primary vertex within 2 cm in the  $z$  direction. The primary vertex is required to lie within  $|z| < 40 \text{ cm}$  from the center of the detector.
2. The muon must lie within a region of the muon detector with high trigger and reconstruction efficiencies, including  $|\eta_{\text{det}}| < 1.6$  (or  $1.6 < |\eta_{\text{det}}| < 2$  for events satisfying the appropriate triggers), where  $|\eta_{\text{det}}|$  is the pseudorapidity measured from the center of the detector.
3. The muon must be isolated in the calorimeter and the central tracker. The total transverse momentum of tracks in a cone of radius  $R = 0.5$  in  $\eta, \phi$  centered around the muon must be less than 2.5 GeV, and the total transverse energy measured in the calorimeter in the annulus  $0.1 < R < 0.4$  centered around the muon track must be less than 2.5 GeV.
4. Missing transverse energy of the event must satisfy  $\cancel{E}_T > 20 \text{ GeV}$ , after being corrected for the muon  $p_T$ .
5. Transverse mass of the  $W$  boson  $M_T > 40 \text{ GeV}$ .
6. Cosmic ray muons are rejected using timing cuts.
7.  $Z \rightarrow \mu\mu$  events are removed by rejecting events containing a second muon crossing three layers of the muon system or if there is a second central track with  $p_T > 20 \text{ GeV}$  and back to back with the muon track in  $\phi$ ,  $|\Delta\phi(\text{muon track, second track})| > 2.1$ .

For  $|\eta_{\text{det}}| < 1.6$ , we selected 594203  $W \rightarrow \mu\nu$  candidates for Run IIa, and 1709325  $W \rightarrow \mu\nu$  for Run IIb. For  $1.6 < |\eta_{\text{det}}| < 2$ , 5950  $W \rightarrow \mu\nu$  candidates from Run IIa were selected.

### IV. BACKGROUNDS

The main backgrounds in the analysis are the multijet background and the electroweak background. The multijet background comes from semileptonic heavy flavor decays. The electroweak background is due to the processes  $W \rightarrow \tau\nu$ ,  $Z \rightarrow \mu\mu$ , and  $Z \rightarrow \tau\tau$ .

## A. Multijet background

The multijet background was estimated from data. The isolation requirement effectively rejects most of the muons from the multijet background. We define  $f$  and  $\epsilon$  as the probabilities for multijet background and for signal events to pass the isolation condition, respectively. These isolation probabilities are used to estimate the multijet background.

To measure  $f$ , we use events with  $\cancel{E}_T < 10$  GeV satisfying all other signal requirements except the isolation condition. To further suppress  $W$  boson production in this sample, events are also required to contain one reconstructed jet with  $p_T > 15$  GeV. The background isolation efficiency is then the ratio between the number of events passing the isolation condition and the total number of selected muon+jet events.

The average isolation efficiency for the multijet background is  $(5.08 \pm 0.2)\%$  [ $(6.13 \pm 0.1)\%$ ] for Run IIa (Run IIb).  $f$  depends on both muon  $p_T$  and  $|\eta|$ , and these dependences were taken into account.

To estimate the systematic uncertainty of the background isolation rate, we add conditions intended to further reduce the contamination from the  $W \rightarrow \mu\nu$  signal and find the systematic uncertainty to be about  $0.71\%$  ( $0.63\%$ ) of  $f$  for Run IIa (Run IIb).

The signal isolation efficiency,  $\epsilon$ , was measured using a sample of dimuon events. The dimuon events were required to pass one of the single muon triggers used for signal events or a dimuon trigger. One of the muons must pass all of the signal muon criteria and, if the event was collected using a single muon trigger, it must match the trigger muon. The second muon must also satisfy all of the signal muon requirements, except for the isolation condition. In addition, the two muons must carry opposite charge, be separated in  $\phi$ , be balanced in  $p_T$ , and have an invariant mass consistent with that of the  $Z$  boson.

The average signal isolation efficiency is  $(93.3 \pm 0.3)\%$  [ $(88.7 \pm 0.3)\%$ ] for Run IIa [Run IIb]. As with  $f$ ,  $\epsilon$  depends on muon  $p_T$  and  $|\eta|$ , and these dependences were taken into account. In addition,  $\epsilon$  was determined separately for positive and negative muons and found to be consistent between the two.

To determine the systematic uncertainty on  $\epsilon$ , the invariant mass range is further restricted to reduce the number of background events, and  $\epsilon$  recalculated. We also add  $0.5\%$  systematic uncertainty from the measurement method. The systematic uncertainty on  $\epsilon$  is  $0.62\%$  ( $0.61\%$ ) for Run IIa (Run IIb).

For  $|\eta_{\text{det}}| < 1.6$ , the background and signal isolation efficiencies were measured independently in  $|\eta|$  and  $p_T$ . For  $1.6 < |\eta_{\text{det}}| < 2$ , due to the low number of available events, the background and signal efficiencies as well as the multijet background were estimated in  $\eta$  bins only. Overall, the multijet background contributes  $(2 \pm 0.1)\%$  [ $(2.4 \pm 0.1)\%$ ] to the Run IIa [Run IIb] data sample.

## B. Electroweak background

A more significant background is due to the processes  $Z/\gamma \rightarrow \mu\mu$ , where one of the muons is mis-reconstructed, and  $W \rightarrow \tau\nu$  and  $Z/\gamma \rightarrow \tau\tau$ , where the tau lepton decays to a muon and a neutrino. This background is estimated using Monte Carlo (MC) samples following the same procedure as was used to reconstruct the  $W \rightarrow \mu\nu$  signal. We use GEANT MC samples generated with PYTHIA.

The momenta of MC muons are smeared to have similar resolution in the data and MC. MC samples are also corrected for efficiencies, the luminosity profile, and the beam shape. The MC samples are normalized to be comparable to the luminosities of the data,  $1037.75 \text{ pb}^{-1}$  ( $3881.78 \text{ pb}^{-1}$ ) for Run IIa (Run IIb). The cross section of the  $W$  boson used is at next-to-next-to-leading-order (NNLO), and those of the  $Z$  boson are at leading-order from PYTHIA, so we apply a K-factor to correct the cross sections of the  $Z$  boson to NNLO.

The systematic uncertainty in the electroweak background is estimated from the variation of the smearing parameters by one standard deviation. The overall electroweak background is  $(3 \pm 0.02)\%$  [ $(3 \pm 0.03)\%$ ] from  $W \rightarrow \tau\nu$ ,  $(2.7 \pm 0.01)\%$  [ $(3.1 \pm 0.01)\%$ ] from  $Z \rightarrow \mu\mu$ , and  $(0.16 \pm 0.001)\%$  [ $(0.18 \pm 0.002)\%$ ] from  $Z \rightarrow \tau\tau$  for Run IIa [Run IIb]. The numbers are given as the percentages of the selected events. We also added the systematic uncertainties from the luminosity and the cross section to the total EW background. The uncertainty is dominated by the statistical uncertainty. The systematic uncertainty from changing the smearing factors is small. In both Run IIa and Run IIb, the background from  $W \rightarrow \tau\nu$  ( $Z \rightarrow \mu\mu$ ) is dominant for  $p_T > 20$  GeV and  $20 < p_T < 35$  GeV ( $p_T > 35$  GeV), and the  $Z \rightarrow \tau\tau$  background is insignificant. The sum of all backgrounds and MC  $W \rightarrow \mu\nu$  agrees with the data.

## V. MUON CHARGE ASYMMETRY

### A. Calculating the muon charge asymmetry

The muon charge asymmetry is calculated as

$$A(\eta) = \frac{N_\mu^+(\eta) - N_\mu^-(\eta)}{N_\mu^+(\eta) + N_\mu^-(\eta)} \quad (7)$$

where  $N_\mu^+$  and  $N_\mu^-$  are the true numbers of positive and negative muons from  $W \rightarrow \mu\nu$  events. Determining the true numbers of positive and negative muon events requires taking not only the backgrounds into account, but also the overall signal efficiency and the muon charge misidentification probability.

In terms of the true numbers of muon events from  $W \rightarrow \mu\nu$  events, after background subtraction, the observed number of muon events is

$$N^\pm = \varepsilon(1 - g)N_\mu^\pm + \varepsilon g N_\mu^\mp \quad (8)$$

where  $N^+$  ( $N^-$ ) is the number of observed positive (negative) muon events,  $\varepsilon$  is the overall signal efficiency, and  $g$  is the probability that a positive (negative) muon is misidentified as a negative (positive) muon. Assuming that the multijet background is independent of muon charge,  $N^\pm$  can also be written as

$$N^\pm = N_{\text{data}}^\pm - N_{\text{EW}}^\pm - \frac{1}{2}N_{\text{MJ}} \quad (9)$$

where  $N_{\text{data}}^\pm$  is the number of selected muons,  $N_{\text{EW}}^\pm$  is the number of muons from electroweak backgrounds, and  $N_{\text{MJ}}$  is the number of muons from multijet background that pass the isolation requirement.

From Eqs. (7) to (9), the muon charge asymmetry can be written as

$$A(\eta) = \frac{1}{(1 - 2g)} \left[ \frac{N^+(\eta) - N^-(\eta)}{N^+(\eta) + N^-(\eta)} \right] \quad (10)$$

The uncertainty in the asymmetry is a quadrature sum of the partial uncertainties from  $N_{\text{data}}^\pm$ ,  $N_{\text{EW}}$ ,  $N_{\text{MJ}}$ , and  $g$ . Each partial uncertainty was determined using the product of an individual variable's uncertainty and the partial derivative of  $A$  with respect to that variable.

The charge misidentification probability,  $g$ , was measured using a sample of dimuon events consistent with being  $Z$  bosons. The charge misidentification probability is the ratio of the number of events in which the two muons have the same sign to the total number of events.

The DØ detector measures muon charge very well. There are only 3 same-sign events out of 48452 events in Run IIa, and 14 same-sign events out of 120417 in Run IIb, making the charge misidentification essentially insignificant. To avoid fluctuations in  $g$  between  $\eta$  and  $p_T$  bins, we set  $g = 0$  and include a systematic uncertainty to account for any bias.

### B. Measuring the muon charge asymmetry

The muon charge asymmetry is calculated (within  $\eta$  bins) using Eq. (10) for three muon  $p_T$  regions:  $p_T > 20$  GeV,  $20 < p_T < 35$  GeV, and  $p_T > 35$  GeV. The background and signal isolation efficiencies are also measured independently in  $\eta$  and  $p_T$  bins. The multijet background is projected from two dimensional distributions in  $p_T$  and  $\eta$  to one dimensional distributions in  $\eta$  for the three  $p_T$  bins. The EW background is also estimated as a function of  $\eta$  for the three  $p_T$  bins.

The asymmetries of Run IIa are consistent with those of Run IIb in all muon  $p_T$  bins. The  $\chi^2/\text{dof}$  are 1 for  $p_T > 20$  GeV, 1.5 for  $20 < p_T < 35$  GeV, and 0.74 for  $p_T > 35$  GeV.

### C. Detector Correction

To compare the measured muon charge asymmetry to the theory prediction, we must correct the asymmetry for detector effects. We use a GEANT MC  $W \rightarrow \mu\nu$  sample generated with PYTHIA to estimate the effect on the asymmetry due to the DØ detector.

The correction is the difference between the asymmetries determined at the generator level and at the detector level. The generator level events are required to have  $p_{T,\nu} > 20$  GeV and are divided into the same muon  $p_T$  bins as the asymmetry measurement. At the detector level, the momentum resolution of MC muons is smeared to match that of data. The detector level events, with no generator level cuts, must pass all of the data selection requirements.

All the corrections for MC samples described in Sec. IV B are done for MC at the detector level. To improve the agreement between the data and MC, we apply a scale factor for the muon distributions in  $\eta$  and  $p_T$  regardless of the charge of the muons. The MC distributions of both types of muons well agree with data.

We use third order polynomial functions to fit the muon charge asymmetries at the generation level and the detector level. The difference between the two fit curves then is used to correct the asymmetry from the data. Figure 2 shows the comparison of the two MC asymmetries and their fit functions for  $p_T > 20$  GeV,  $20 < p_T < 35$  GeV, and  $p_T > 35$  GeV.

The systematic uncertainty of the detector correction is estimated by changing the fit range. We also change the smearing factors by one standard deviation to estimate the systematic uncertainty of the difference.

Figure 3 displays the corrected asymmetries with  $p_T > 20$  GeV,  $20 < p_T < 35$  GeV, and  $p_T > 35$  GeV for Run IIa (blue) and Run IIb (red). The brown central line is the CTEQ6.6 prediction. The yellow band is drawn from the 44 CTEQ6.6 uncertainty sets. The theoretical prediction is based on RESBOS [1] using the CTEQ6.6 PDFs and PHOTOS [2] for the modeling of final state radiation. The theoretical curves are generated by requiring a 20 GeV cut on the muon and neutrino traverse momentum in the generation level. The PDF uncertainty band is calculated using the method described in Ref. [4]

#### D. Magnet directions

In the DØ detector, the regular reversal of the solenoid and toroid polarities helps cancel detector asymmetries. We checked the effects of solenoid and toroid polarities by calculating the raw asymmetries for four subsets of data with different magnetic field polarities: forward toroid and forward solenoid, forward toroid and reverse solenoid, reverse toroid and forward solenoid, reverse toroid and reverse solenoid. Each combination contributes between 22% and 28% of the Run IIa and Run IIb data sets. All asymmetries are in good agreement.

#### E. CP folding

The muon charge asymmetry should be symmetric under CP folding. We confirm this by calculating that  $A(\eta)$  is consistent with  $-A(-\eta)$  for all  $p_T$  bins and data sets.

The CP folded asymmetry is calculated by

- adding the numbers of positive and negative muons for data and electroweak backgrounds,  $N_{\text{CP}}^{\pm} = N^{\pm}(\eta) + N^{\mp}(-\eta)$ ,
- re-calculating the background isolation efficiency, signal isolation efficiency, multijet background, and muon charge misidentification probability after folding the  $\pm|\eta|$  bins,
- and recalculating all statistical uncertainties.

### VI. COMBINED RESULTS FOR RUN IIA AND RUN IIB

The combined asymmetry is the weighted mean of the asymmetries of Run IIa and Run IIb. The combined CP folded asymmetries are shown in Fig. 4. For  $0.6 < |\eta| < 1.6$ , the total uncertainties are smaller than the PDF uncertainty band in most of the  $\eta$  bins. Tables I to III show measured values of the combined and CP-folded results.

#### A. Muon and electron channel comparison

To have comparable results with the DØ electron charge asymmetry [3], we repeat the analysis with the following kinematic cuts:

- $p_{T,\mu} > 25$  GeV,
- $\cancel{E}_T > 25$  GeV,

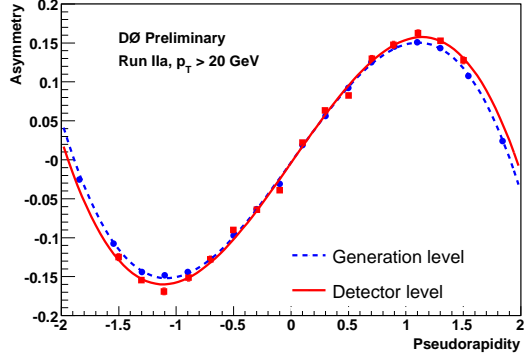
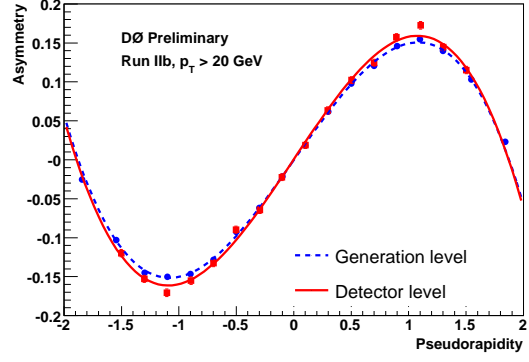
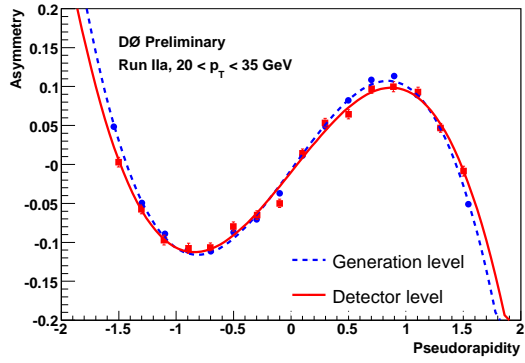
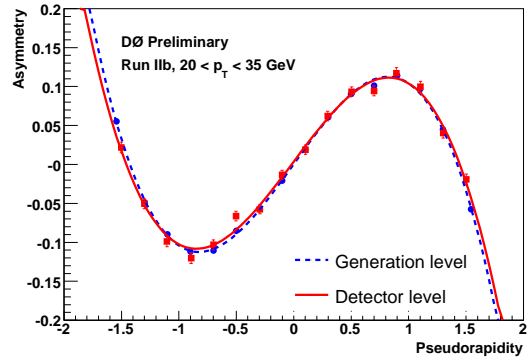
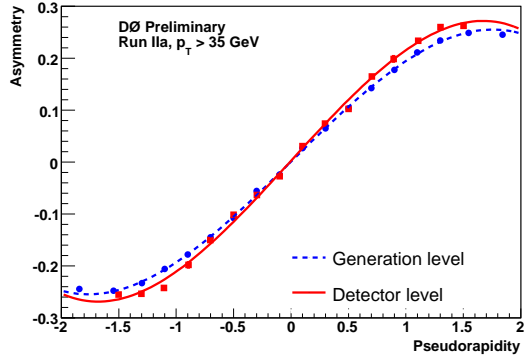
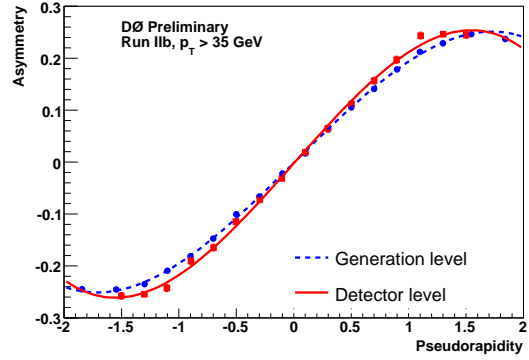
(a) Run IIa,  $p_T > 20$  GeV(b) Run IIb,  $p_T > 20$  GeV(c) Run IIa,  $20 < p_T < 35$  GeV(d) Run IIb,  $20 < p_T < 35$  GeV(e) Run IIa,  $p_T > 35$  GeV(f) Run IIb,  $p_T > 35$  GeV

FIG. 2: Comparison of muon charge asymmetry as a function of  $\eta$  between MC at the generation level (blue) and detector level (red) for Run IIa and Run IIb, for  $p_T > 20$  GeV,  $20 < p_T < 35$  GeV, and  $p_T > 35$  GeV.

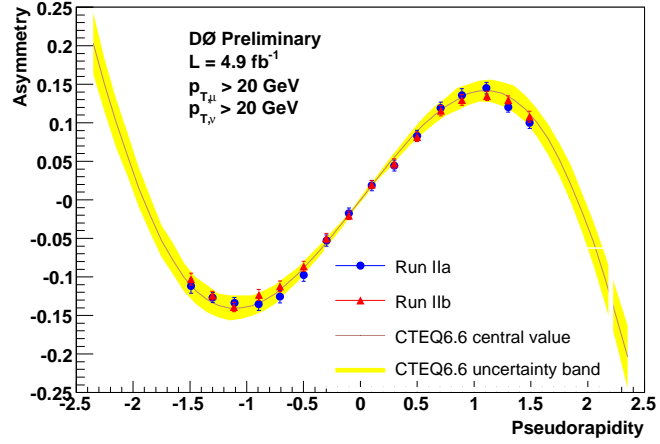
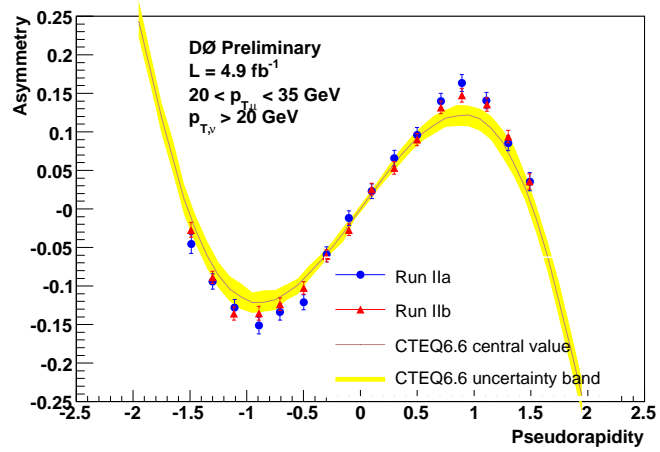
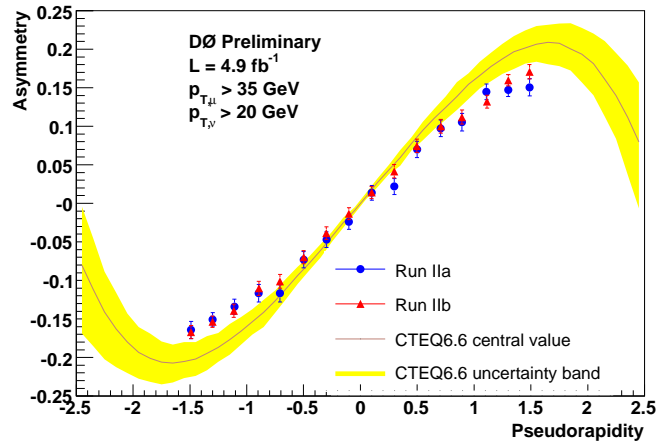
(a)  $p_{T,\mu} > 20 \text{ GeV}$ ,  $p_{T,\nu} > 20 \text{ GeV}$ (b)  $20 < p_{T,\mu} < 35 \text{ GeV}$ ,  $p_{T,\nu} > 20 \text{ GeV}$ (c)  $p_{T,\mu} > 35 \text{ GeV}$ ,  $p_{T,\nu} > 20 \text{ GeV}$ 

FIG. 3: Corrected muon charge asymmetry as a function of pseudorapidity for  $p_T > 20 \text{ GeV}$ ,  $20 < p_T < 35 \text{ GeV}$ , and  $p_T > 35 \text{ GeV}$  for Run IIa and Run IIb. The brown line and yellow band are the central line and error band of CTEQ6.6 prediction.

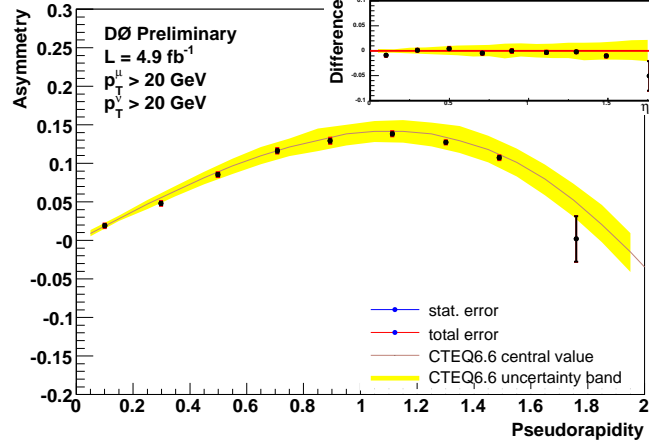
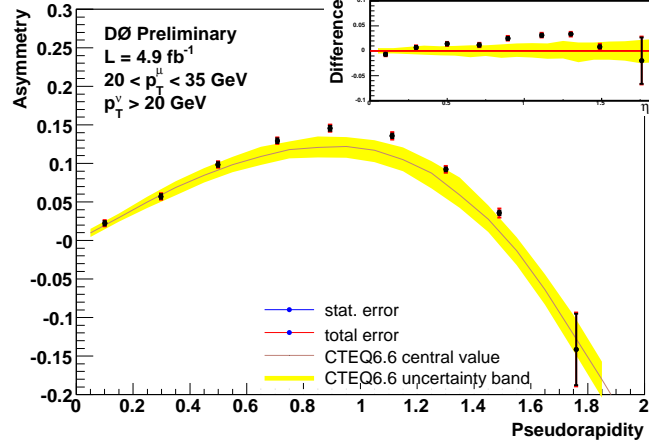
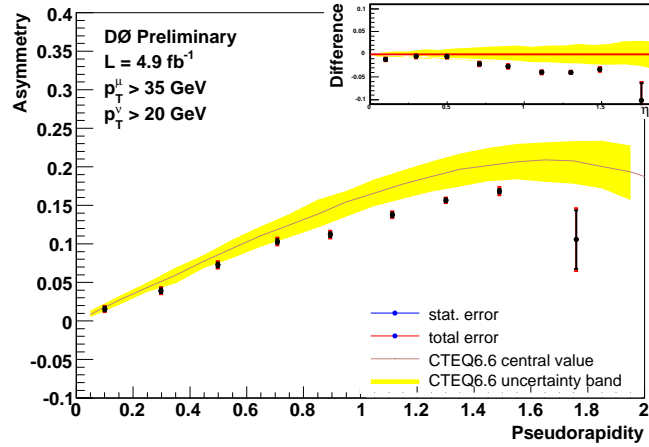
(a)  $p_{T,\mu} > 20 \text{ GeV}$ ,  $p_{T,\nu} > 20 \text{ GeV}$ (b)  $20 < p_{T,\mu} < 35 \text{ GeV}$ ,  $p_{T,\nu} > 20 \text{ GeV}$ (c)  $p_{T,\mu} > 35 \text{ GeV}$ ,  $p_{T,\nu} > 20 \text{ GeV}$ 

FIG. 4: Combined CP folded muon charge asymmetry as a function of pseudorapidity for  $p_T > 20 \text{ GeV}$ ,  $20 < p_T < 35 \text{ GeV}$ , and  $p_T > 35 \text{ GeV}$ . The brown line and yellow band are the central line and error band of CTEQ6.6 prediction. The top right windows show the difference between the muon charge asymmetry and the central value of CTEQ66.

$\eta$ bin	$\langle \eta \rangle$	$A_{\text{CP folded}}^*$	stat.	sys.
0.00-0.20	0.10	0.0190	0.0020	0.0021
0.20-0.40	0.30	0.0480	0.0021	0.0023
0.40-0.60	0.50	0.0854	0.0021	0.0027
0.60-0.80	0.71	0.1162	0.0022	0.0031
0.80-1.00	0.89	0.1292	0.0023	0.0033
1.00-1.20	1.11	0.1383	0.0020	0.0029
1.20-1.40	1.30	0.1273	0.0017	0.0023
1.40-1.70	1.49	0.1073	0.0020	0.0027
1.70-2.00	1.76	0.0019	0.0294	0.0059

TABLE I: Combined Run IIa and Run IIb CP folded asymmetry for  $p_T > 20$  GeV:  $\eta$  bin, average  $\eta$  ( $\langle \eta \rangle$ ), combined corrected CP folded asymmetry ( $A_{\text{CP folded}}^*$ ), statistical uncertainty (stat.), systematic uncertainty (sys.).

$\eta$ bin	$\langle \eta \rangle$	$A_{\text{CP folded}}^*$	stat.	sys.
0.00-0.20	0.10	0.0224	0.0028	0.0029
0.20-0.40	0.30	0.0571	0.0030	0.0031
0.40-0.60	0.50	0.0985	0.0029	0.0031
0.60-0.80	0.71	0.1294	0.0031	0.0031
0.80-1.00	0.89	0.1457	0.0032	0.0035
1.00-1.20	1.11	0.1358	0.0029	0.0038
1.20-1.40	1.30	0.0922	0.0024	0.0038
1.40-1.70	1.49	0.0357	0.0029	0.0050
1.70-2.00	1.76	-0.1414	0.0462	0.0129

TABLE II: Combined Run IIa and Run IIb CP folded asymmetry for  $20 < p_T < 35$  GeV:  $\eta$  bin, average  $\eta$  ( $\langle \eta \rangle$ ), combined corrected CP folded asymmetry ( $A_{\text{CP folded}}^*$ ), statistical uncertainty (stat.), systematic uncertainty (sys.).

$\eta$ bin	$\langle \eta \rangle$	$A_{\text{CP folded}}^*$	stat.	sys.
0.00-0.20	0.10	0.0156	0.0029	0.0031
0.20-0.40	0.30	0.0392	0.0030	0.0035
0.40-0.60	0.50	0.0727	0.0030	0.0038
0.60-0.80	0.71	0.1030	0.0031	0.0040
0.80-1.00	0.89	0.1121	0.0032	0.0040
1.00-1.20	1.11	0.1379	0.0028	0.0036
1.20-1.40	1.30	0.1565	0.0024	0.0030
1.40-1.70	1.49	0.1684	0.0028	0.0047
1.70-2.00	1.76	0.1056	0.0379	0.0151

TABLE III: Combined Run IIa and Run IIb CP folded asymmetry for  $p_T > 35$  GeV:  $\eta$  bin, average  $\eta$  ( $\langle \eta \rangle$ ), combined corrected CP folded asymmetry ( $A_{\text{CP folded}}^*$ ), statistical uncertainty (stat.), systematic uncertainty (sys.).

- $M_T > 50$  GeV.

The  $\eta$  bin size is also changed to that of electron channel. Figure 5 shows the comparison of the muon charge asymmetry to the electron charge asymmetry, the CTEQ6.6 prediction, and the MRST04NLO prediction [5]. The electron charge asymmetry is consistent with the muon charge asymmetry. The  $\chi^2/\text{dof}$  comparing the electron and muon charge asymmetries are 1.2, 1.1 and 3.6 for  $p_{T,\ell} > 25$  GeV,  $25 < p_{T,\ell} < 35$  GeV, and  $p_{T,\ell} > 35$  GeV, respectively. Except in the highest  $\eta_\mu$  bin, the uncertainty in the muon channel is smaller than the uncertainty in the electron channel. Tables IV to VI show the muon charge asymmetry, the electron charge asymmetry, the CTEQ6.6 prediction and the MRST04NLO for the three  $p_T$  bins.

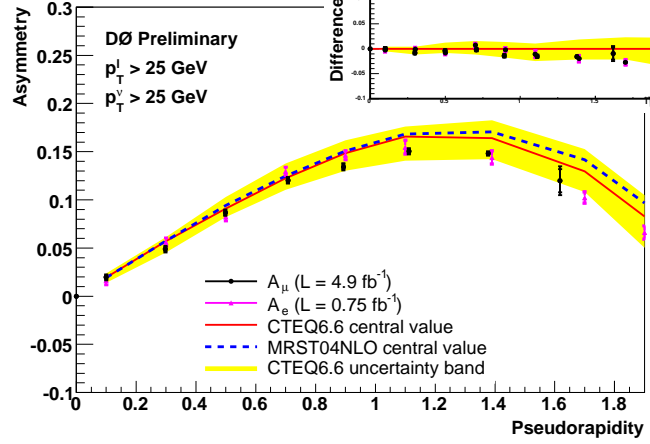
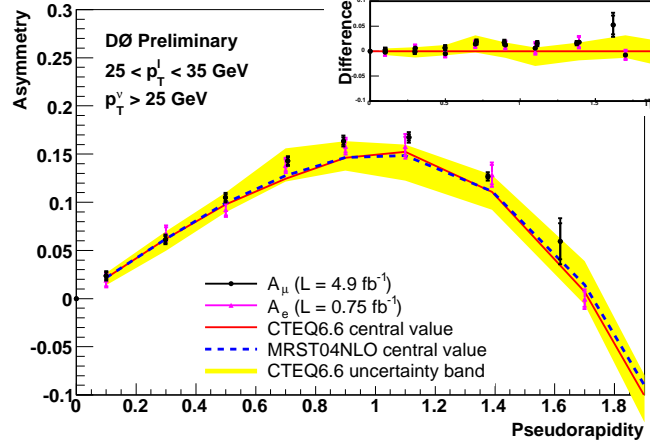
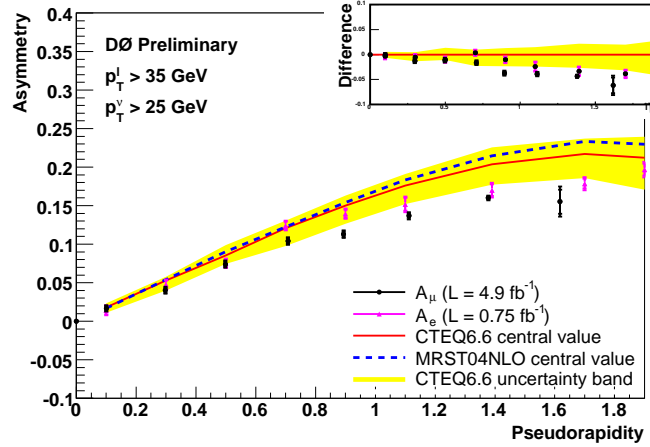
(a)  $p_{T,\ell} > 25 \text{ GeV}, p_{T,\nu} > 25 \text{ GeV}$ (b)  $25 < p_{T,\ell} < 35 \text{ GeV}, p_{T,\nu} > 25 \text{ GeV}$ (c)  $p_{T,\ell} > 35 \text{ GeV}, p_{T,\nu} > 25 \text{ GeV}$ 

FIG. 5: Comparison of the muon charge asymmetry (black) and the electron charge asymmetry (pink) for (top)  $p_{T,\ell} > 25 \text{ GeV}$ , (center)  $25 < p_{T,\ell} < 35 \text{ GeV}$ , and (bottom)  $p_{T,\ell} > 35 \text{ GeV}$ . The red line is the central value of CTEQ6.6. The yellow band is the uncertainty band of the CTEQ6.6 prediction. The blue dashed line is the prediction of MRST04NLO. The top right windows show the difference between the muon charge asymmetry and the central value of CTEQ6.6.

$\eta$ bin	$\langle \eta_\mu \rangle$	$A_\mu \pm \text{stat.} \pm \text{sys.}$	$A_e \pm \text{stat.} \pm \text{sys.}$	$A_{\text{CT}}^{+\text{upper error}}_{-\text{lower error}}$	$A_{\text{MR}}$
0.00-0.20	0.10	$0.0196 \pm 0.0022 \pm 0.0023$	$0.0163 \pm 0.0040 \pm 0.0028$	$0.0193^{+0.0043}_{-0.0054}$	0.0191
0.20-0.40	0.30	$0.0489 \pm 0.0023 \pm 0.0024$	$0.0561 \pm 0.0039 \pm 0.0031$	$0.0571^{+0.0044}_{-0.0116}$	0.0575
0.40-0.60	0.50	$0.0867 \pm 0.0023 \pm 0.0025$	$0.0825 \pm 0.0039 \pm 0.0030$	$0.0910^{+0.0120}_{-0.0087}$	0.0943
0.60-0.80	0.71	$0.1203 \pm 0.0024 \pm 0.0025$	$0.1296 \pm 0.0038 \pm 0.0030$	$0.1223^{+0.0155}_{-0.0118}$	0.1247
0.80-1.00	0.89	$0.1343 \pm 0.0024 \pm 0.0027$	$0.1464 \pm 0.0042 \pm 0.0034$	$0.1483^{+0.0133}_{-0.0181}$	0.1506
1.00-1.20	1.11	$0.1504 \pm 0.0022 \pm 0.0025$	$0.1548 \pm 0.0064 \pm 0.0048$	$0.1656^{+0.0105}_{-0.0249}$	0.1682
1.20-1.60	1.38	$0.1481 \pm 0.0014 \pm 0.0019$	$0.1441 \pm 0.0061 \pm 0.0047$	$0.1640^{+0.0185}_{-0.0217}$	0.1706
1.60-1.80	1.62	$0.1198 \pm 0.0120 \pm 0.0088$	$0.1024 \pm 0.0050 \pm 0.0044$	$0.1296^{+0.0231}_{-0.0215}$	0.1418

TABLE IV: Compare  $A_\mu$ ,  $A_e$ ,  $A_{\text{CTEQ66}}$ , and  $A_{\text{MRST04NLO}}$  for  $p_{T,\ell} > 25$  GeV,  $p_{T,\nu} > 25$  GeV:  $\eta$  bin, average  $\eta$  ( $\langle \eta_\mu \rangle$ ), muon charge asymmetry ( $A_\mu \pm \text{stat.} \pm \text{sys.}$ ), electron charge asymmetry ( $A_e \pm \text{stat.} \pm \text{sys.}$ ), theory prediction from CTEQ6.6 with upper and lower errors ( $A_{\text{CT}}^{+\text{upper error}}_{-\text{lower error}}$ ), and prediction from MRST04NLO ( $A_{\text{MR}}$ ).

$\eta$ bin	$\langle \eta_\mu \rangle$	$A_\mu \pm \text{stat.} \pm \text{sys.}$	$A_e \pm \text{stat.} \pm \text{sys.}$	$A_{\text{CT}}^{+\text{upper error}}_{-\text{lower error}}$	$A_{\text{MR}}$
0.00-0.20	0.10	$0.0237 \pm 0.0034 \pm 0.0036$	$0.0193 \pm 0.0062 \pm 0.0045$	$0.0212^{+0.0054}_{-0.0075}$	0.0218
0.20-0.40	0.30	$0.0615 \pm 0.0036 \pm 0.0037$	$0.0678 \pm 0.0061 \pm 0.0052$	$0.0621^{+0.0076}_{-0.0126}$	0.0619
0.40-0.60	0.50	$0.1047 \pm 0.0035 \pm 0.0038$	$0.0925 \pm 0.0060 \pm 0.0049$	$0.0978^{+0.0122}_{-0.0081}$	0.0994
0.60-0.80	0.71	$0.1428 \pm 0.0036 \pm 0.0037$	$0.1384 \pm 0.0061 \pm 0.0052$	$0.1245^{+0.0314}_{-0.0030}$	0.1277
0.80-1.00	0.89	$0.1636 \pm 0.0038 \pm 0.0041$	$0.1584 \pm 0.0067 \pm 0.0057$	$0.1461^{+0.0172}_{-0.0133}$	0.1464
1.00-1.20	1.11	$0.1674 \pm 0.0033 \pm 0.0043$	$0.1580 \pm 0.0100 \pm 0.0082$	$0.1523^{+0.0074}_{-0.0299}$	0.1484
1.20-1.60	1.38	$0.1268 \pm 0.0022 \pm 0.0038$	$0.1287 \pm 0.0101 \pm 0.0079$	$0.1108^{+0.0175}_{-0.0185}$	0.1114
1.60-1.80	1.62	$0.0595 \pm 0.0188 \pm 0.0149$	$-0.0006 \pm 0.0079 \pm 0.0064$	$0.0069^{+0.0318}_{-0.0133}$	0.0141

TABLE V: Compare  $A_\mu$ ,  $A_e$ ,  $A_{\text{CTEQ66}}$ , and  $A_{\text{MRST04NLO}}$  for  $25 < p_{T,\ell} < 35$  GeV,  $p_{T,\nu} > 25$  GeV:  $\eta$  bin, average  $\eta$  ( $\langle \eta_\mu \rangle$ ), muon charge asymmetry ( $A_\mu \pm \text{stat.} \pm \text{sys.}$ ), electron charge asymmetry ( $A_e \pm \text{stat.} \pm \text{sys.}$ ), theory prediction from CTEQ6.6 with upper and lower errors ( $A_{\text{CT}}^{+\text{upper error}}_{-\text{lower error}}$ ), and prediction from MRST04NLO ( $A_{\text{MR}}$ ).

$\eta$ bin	$\langle \eta_\mu \rangle$	$A_\mu \pm \text{stat.} \pm \text{sys.}$	$A_e \pm \text{stat.} \pm \text{sys.}$	$A_{\text{CT}}^{+\text{upper error}}_{-\text{lower error}}$	$A_{\text{MR}}$
0.00-0.20	0.10	$0.0167 \pm 0.0029 \pm 0.0031$	$0.0143 \pm 0.0052 \pm 0.0036$	$0.0178^{+0.0053}_{-0.0067}$	0.0169
0.20-0.40	0.30	$0.0402 \pm 0.0031 \pm 0.0033$	$0.0477 \pm 0.0051 \pm 0.0037$	$0.0530^{+0.0045}_{-0.0133}$	0.0540
0.40-0.60	0.50	$0.0742 \pm 0.0030 \pm 0.0035$	$0.0752 \pm 0.0050 \pm 0.0036$	$0.0855^{+0.0132}_{-0.0109}$	0.0903
0.60-0.80	0.71	$0.1042 \pm 0.0031 \pm 0.0036$	$0.1242 \pm 0.0049 \pm 0.0036$	$0.1206^{+0.0097}_{-0.0231}$	0.1224
0.80-1.00	0.89	$0.1130 \pm 0.0032 \pm 0.0037$	$0.1395 \pm 0.0054 \pm 0.0040$	$0.1501^{+0.0131}_{-0.0237}$	0.1539
1.00-1.20	1.11	$0.1369 \pm 0.0028 \pm 0.0035$	$0.1518 \pm 0.0083 \pm 0.0059$	$0.1759^{+0.0150}_{-0.0239}$	0.1833
1.20-1.60	1.38	$0.1602 \pm 0.0018 \pm 0.0025$	$0.1701 \pm 0.0077 \pm 0.0056$	$0.2038^{+0.0217}_{-0.0265}$	0.2147
1.60-1.80	1.62	$0.1552 \pm 0.0156 \pm 0.0115$	$0.1785 \pm 0.0063 \pm 0.0055$	$0.2171^{+0.0198}_{-0.0315}$	0.2333

TABLE VI: Compare  $A_\mu$ ,  $A_e$ ,  $A_{\text{CTEQ66}}$ , and  $A_{\text{MRST04NLO}}$  for  $p_{T,\ell} > 35$  GeV,  $p_{T,\nu} > 25$  GeV:  $\eta$  bin, average  $\eta$  ( $\langle \eta_\mu \rangle$ ), muon charge asymmetry ( $A_\mu \pm \text{stat.} \pm \text{sys.}$ ), electron charge asymmetry ( $A_e \pm \text{stat.} \pm \text{sys.}$ ), theory prediction from CTEQ6.6 with upper and lower errors ( $A_{\text{CT}}^{+\text{upper error}}_{-\text{lower error}}$ ), and prediction from MRST04NLO ( $A_{\text{MR}}$ ).

## VII. CONCLUSION

We have measured the muon charge asymmetry from  $W \rightarrow \mu\nu$  decay for  $|\eta| < 2$  using  $4.9 \text{ fb}^{-1}$  of data collected with  $D\bar{O}$  detector and compared our result with the prediction from the CTEQ6.6 PDF set. The total uncertainties are smaller than the PDF uncertainties in most  $\eta$  bins. Comparison between the muon channel and the electron channel shows that the two results are consistent in all three  $p_T$  bins. The total uncertainty in the muon channel is smaller than that of electron channel.

### Acknowledgments

We thank the staffs at Fermilab and collaborating institutions, and acknowledge support from the DOE and NSF (USA); CEA and CNRS/IN2P3 (France); FASI, Rosatom and RFBR (Russia); CNPq, FAPERJ, FAPESP and FUNDUNESP (Brazil); DAE and DST (India); Colciencias (Colombia); CONACyT (Mexico); KRF and KOSEF (Korea); CONICET and UBACyT (Argentina); FOM (The Netherlands); STFC and the Royal Society (United Kingdom); MSMT and GACR (Czech Republic); CRC Program, CFI, NSERC and WestGrid Project (Canada); BMBF and DFG (Germany); SFI (Ireland); The Swedish Research Council (Sweden); CAS and CNSF (China); and the Alexander von Humboldt Foundation (Germany).

- 
- [1] C. Balazs and C.P. Yuan, Phys. Rev. D **56**, 5558 (1997)
  - [2] E. Barberio and Z. Was, Comput. Phys. Commun. **79**, 291 (1994); we use PHOTOS version 2.0.
  - [3] V. Abazov *et al.* (DØ Collaboration), Phys. Rev. Lett. **101**, 211801 (2008).
  - [4] P.M. Nadolsky *et al.*, Phys. Rev. D **78**, 013004, (2008).
  - [5] A.D. Martin, R.G. Roberts, W.J. Stirling, and R.S. Thorne, Phys. Lett. B **604**, 61 (2004).